Supplemental Material

Test of different anchor points for Figure 1

The choice of the anchor point should not change our conclusions if all experimental results are perfect and if Lindemann's Law applies for the melting of ferropericlase. However, the seven experimental data (Figure 1) are of different quality. We chose the anchor point at around 50 GPa since most experiments by (Deng and Lee, 2017) have been performed at or near this pressure to constrain the phase diagram and the melting temperature at this pressure is presumably best constrained as stated in the main text. In Figure S1, we present the Lindemann's Law prediction using all possible anchor points. Overall, the melting curves based on 3000 K bulk modulus data show the best agreement with the experimental results regardless of the anchor points used.

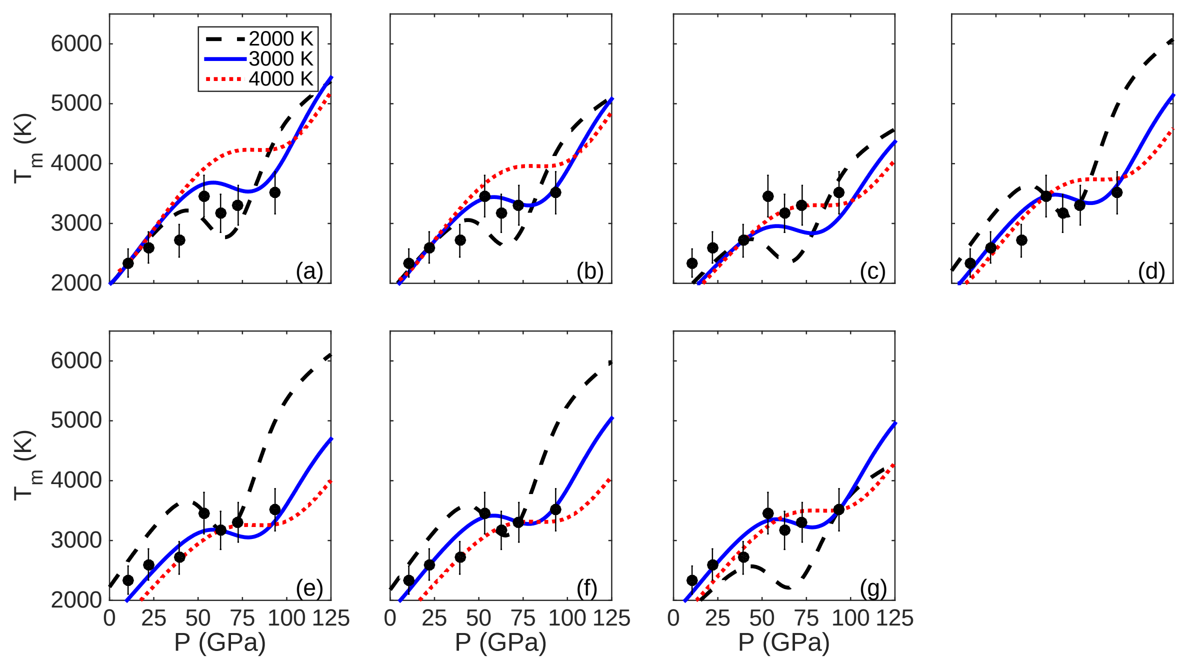

Figure S1. Comparison of ferropericlase melting curves predicted by Lindemann's Law with experimental results (Deng and Lee, 2017; Du and Lee, 2014). (a)-(g) show the melting curves of (Mg,Fe)O predicted by Lindemann's Law with reference point at 10, 22, 39, 53, 63, 72, and 93 GPa respectively. Note that (d) is the same as shown in Figure 1c in the manuscript.

Melting curves of B-site ferric iron-bearing bridgmanite of predicted by Lindemann's Law

We are aware of the following publications on the thermoelastic properties of B-site ferric iron-bearing bridgmanite at high temperatures and high pressures.

1- $(Mg_{0.875}Fe^{3+}_{0.125})(Si_{0.875}Fe^{3+}_{0.125})O_3$, at 300 and 2000 K (Hsu et al., 2011)
2- $(Mg_{0.9375}Fe^{3+}_{0.0625})(Si_{0.9375}Fe^{3+}_{0.0625})O_3$, at 300, 1000, 2000, 3000, 4000 K (Tsuchiya and Wang, 2013)
3- $(Mg_{0.875}Fe^{3+}_{0.125})(Si_{0.875}Fe^{3+}_{0.125})O_3$, at 300, 1000, 2000, 3000, 4000 K (Shukla and Wentzcovitch, 2016)
4- $(Mg_{0.95}Fe^{3+}_{0.05})(Si_{0.95}Fe^{3+}_{0.05})O_3$ at 300, 700, 1000, 2700, 4000 K (Shukla et al., 2016). Bulk modulus at 4000 K was only presented from 90 GPa and data at lower pressures are not available. But we need data from around 25 GPa to integrate the differential Lindemann equation using the relatively well-constrained melting temperature at 25 GPa as the reference point. Therefore, 4000 K curve is not useful in this study.

Here we calculate the bulk modulus derivative and the melting temperatures based on Lindemann's Law for all the data mentioned above (Figure S2 a-d).

All of the above studies agree that at temperatures > 2000 K, the elastic softening caused by the spin transition of iron is negligibly small and K_T' is larger than 1 at least up to 140 GPa. As a result, the spin transition of iron cannot be the main cause of the flat melting curve of bridgmanite observed by Heinz and Jeanloz (1987) and Knittle and Jeanloz (1989). We also note that the melting curves calculated based on bulk modulus at high temperatures (i.e., 4000 K) are in good agreement with (Zerr and Boehler, 1993) from 25 GPa to 60 GPa.

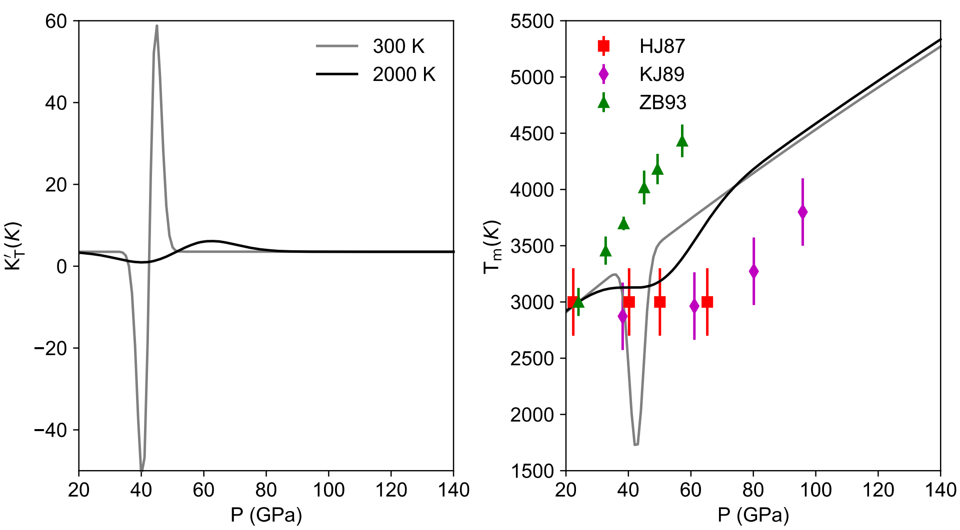

Figure S2a. K_T' (the pressure derivative of bulk modulus) and T_m (the melting temperature) calculated based on the bulk modulus data of $(Mg_{0.875}Fe^{3+}_{0.125})(Si_{0.875}Fe^{3+}_{0.125})O_3$, at 300 and 2000 K by (Hsu et al., 2011). Previous experimentally determined melting temperatures of bridgmanite are also shown ($(Mg_{0.9}Fe_{0.1})SiO_3$ by HJ87 (Heinz and Jeanloz, 1987) (red squares),

$(Mg_{0.88}Fe_{0.12})SiO_3$ by KJ89 (Knittle and Jeanloz, 1989) (purple diamonds), and $(Mg_{0.88}Fe_{0.12})SiO_3$ by ZB93 (Zerr and Boehler, 1993) (green triangles) where the pressures reported already include thermal pressure.

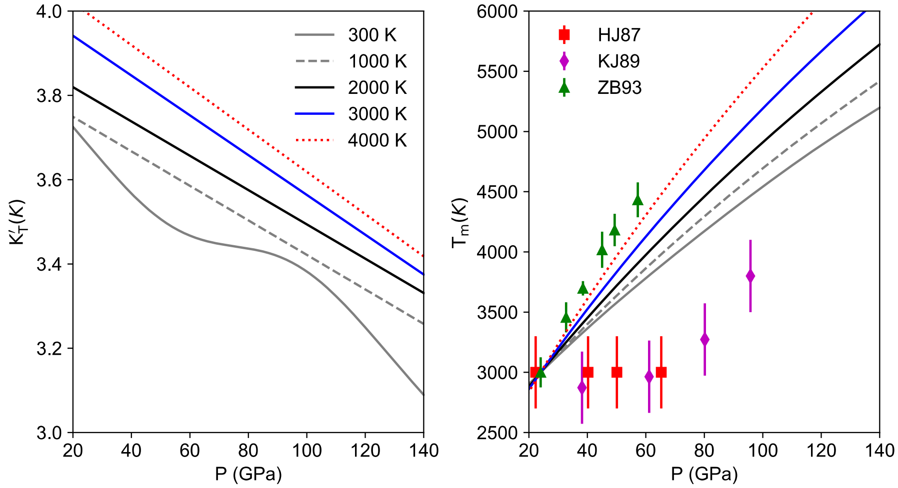

Figure S2b. K_T' and T_m calculated based on the bulk modulus data by (Tsuchiya and Wang, 2013) for $(Mg_{0.9375}Fe^{3+}_{0.0625})(Si_{0.9375}Fe^{3+}_{0.0625})O_3$, at 300, 1000, 2000, 3000, and 4000 K. Tsuchiya and Wang (2013) found very marginal effects of spin transition on the bulk modulus at all temperatures considered. Therefore, the corresponding melting curves do not show any substantial depression as observed for (Mg,Fe)O.

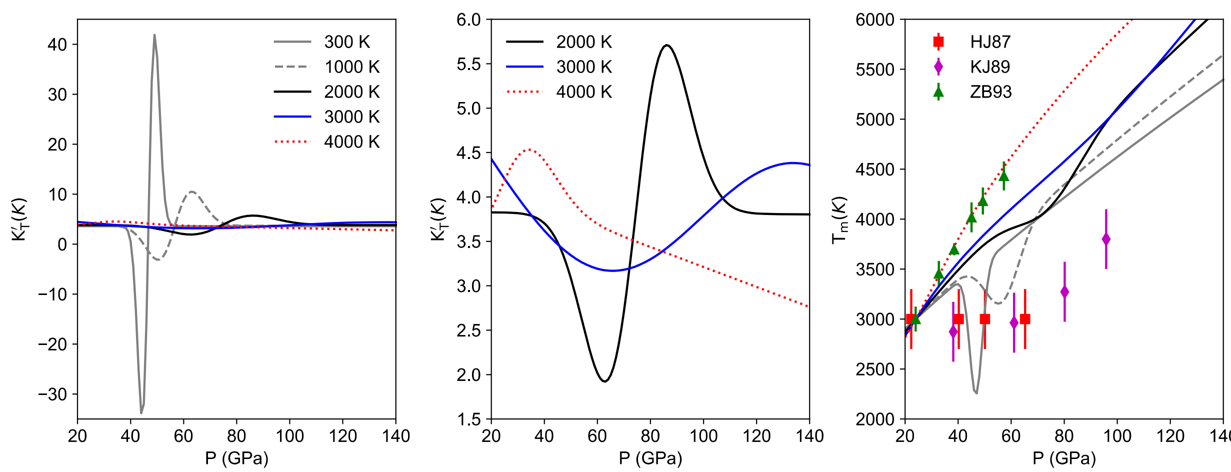

Figure S2c. K_T' and T_m calculated based on the bulk modulus data by (Shukla and Wentzcovitch, 2016) for $(Mg_{0.875}Fe^{3+}_{0.125})(Si_{0.875}Fe^{3+}_{0.125})O_3$, at 300, 1000, 2000, 3000, and 4000 K. The mid-panel only shows K_T' at 2000, 3000, and 4000 K to better scale the figure.

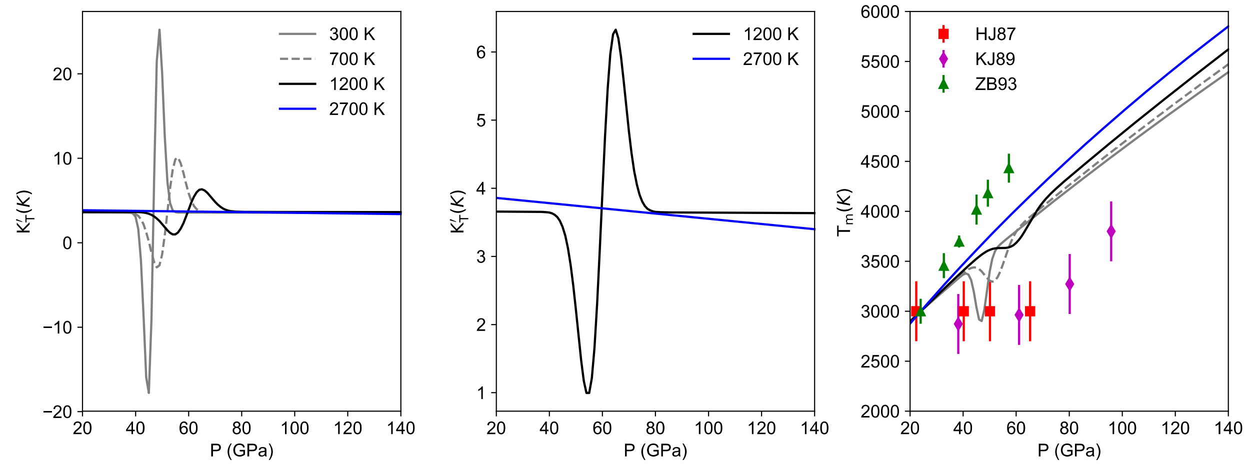

Figure S2d. K_T' and T_m calculated based on the bulk modulus data by (Shukla et al., 2016) for $(Mg_{0.95}Fe^{3+}_{0.05})(Si_{0.95}Fe^{3+}_{0.05})O_3$, at 300, 700, 1000, and 2700 K.

Reference

Heinz, D.L., and Jeanloz, R. (1987) Measurement of the melting curve of Mg0.9Fe0.1SiO3 at lower mantle conditions and its geophysical implications. Journal of Geophysical Research: Solid Earth, 92(B11), 11437-11444.

Hsu, H., Blaha, P., Cococcioni, M., and Wentzcovitch, R.M. (2011) Spin-State Crossover and Hyperfine Interactions of Ferric Iron in $MgSiO_3$ Perovskite. Physical Review Letters, 106(11), 118501.

Knittle, E., and Jeanloz, R. (1989) Melting curve of $(Mg,Fe)SiO_3$ perovskite to 96 GPa: Evidence for a structural transition in lower mantle melts. Geophysical Research Letters, 16(5), 421-424.

Shukla, G., Cococcioni, M., and Wentzcovitch, R.M. (2016) Thermoelasticity of Fe^{3+}- and Al-bearing bridgmanite: Effects of iron spin crossover. Geophysical Research Letters, 43(11), 5661-5670.

Shukla, G., and Wentzcovitch, R.M. (2016) Spin crossover in $(Mg,Fe^{3+})(Si,Fe^{3+})O3$ bridgmanite: Effects of disorder, iron concentration, and temperature. Physics of the Earth and Planetary Interiors, 260, 53-61.

Tsuchiya, T., and Wang, X. (2013) Ab initio investigation on the high-temperature thermodynamic properties of Fe3+-bearing MgSiO3 perovskite. 118(1), 83-91.

Zerr, A., and Boehler, R. (1993) Melting of $(Mg,Fe)SiO_3$-Perovskite to 625 Kilobars - Indication of a High-Melting Temperature in the Lower Mantle. Science, 262(5133), 553-555.